

THE SCALING PROPERTIES OF HIGH-FREQUENCY WIND SPEED RECORDS BASED ON MULTISCALE MULTIFRACTAL ANALYSIS

MING ZENG[†], XIAO-NEI ZHANG, JING-HAI LI, QING-HAO MENG

Institute of Robotics and Autonomous Systems
School of Electrical Engineering and Automation
Tianjin University, Tianjin 300072, China

(Received June 8, 2016; revised version received June 29, 2016)

In this paper, we employ the multiscale multifractal analysis (MMA) method to investigate the fractal properties of wind speed records depending on their magnitude of the fluctuations and the timescale. The MMA results show that the high-frequency wind speed records appear to be far more complex and contain abundant information, which cannot be detected by the popular scaling analysis method, *i.e.*, multifractal detrended fluctuation analysis (MF-DFA). Comparing the Hurst surfaces of nine groups of wind speed data, we find that for the negative qs , all the surfaces exhibit intensive fluctuations and significant differences. In addition, the distribution histograms of Hurst surfaces for the positive qs reveal that the large fluctuations of all wind speed data depend on the spatial positions, which is further illustrated by the wind roses. Subsequent analysis of shuffled and surrogate series reveals that the multifractality of wind speed time series is mainly stemming from the long-range correlation, while has less to do with broad probability density function. Finally, the effect of sampling period is discussed. The results suggest that a sampling period of 20 min is sufficient to characterize multiscale multifractal properties of high-frequency wind speed data.

DOI:10.5506/APhysPolB.47.2205

1. Introduction

Knowledge about the nature of wind speed records has far reaching impact on diverse fields of research, such as energy generation [1], air pollution control [2], civil engineering [3], aeolian sediment transport [4], *etc.* Within the atmospheric boundary layer, due to the interplay among many complex factors including pressure gradient, turbulence, temperature and topography [5], the near-surface wind speed variations exhibit highly irregular

[†] Corresponding author: zengming@tju.edu.cn

fluctuations and complex behaviors. Thus, traditional simulation models accompanied with implicit assumptions, *e.g.*, wind tunnel simulations [6], computational fluid dynamics (CFD) approaches [7], have quite limitations as applied to reveal complex dynamic behaviors of wind field. In this regard, it is imperative for us to get a deeper insight into the fluctuation mechanisms of wind speed for the purpose of modeling, prediction, simulation and design.

The characterization of wind speed records elicits a great deal attention from various research fields. The statistical analysis [8], chaotic time series analysis [9], wavelet analysis [10], power spectral density [11], Hilbert–Huang transform [12], and complexity analysis [13] have been implemented to the investigation of wind fields. In particular, the technique of fractal analysis has already proven its great potential for uncovering scaling properties of wind speed records [14–20]. Kavasseri *et al.* [14, 15] systematically analyzed hourly wind speed data from different wind-generation sites in North Dakota, using the detrended fluctuation analysis (DFA) [21], and its extension, multifractal detrended fluctuation analysis (MF-DFA) [22]. Their results suggest that the hourly wind speed data exhibit similar long-range correlations and a characteristic broad multifractal spectrum irrespective of the geographical location and topography. These features of wind speed records are further confirmed at extensive regions of the world using different station densities and periods by Koçak [16] and Santos *et al.* [17]. Feng *et al.* [18] reported that non-universal multifractal behaviors exist in the long daily wind speed time series from China. Telesca *et al.* [19] analyzed the height dependence of the informational and multifractal properties of hourly wind data. More recently, Telesca *et al.* [20] applied the MF-DFA and power spectrum to six high-frequency records of 10 min averages of wind speed measured in Switzerland, and in all examined cases, they found that the wind speed is persistent and multifractal at larger timescales and antipersistent and monofractal (or weakly multifractal) at smaller ones.

Despite the existing contributions, significant challenges in the study of wind fields remain. Note that the majority of the studies concerning fractal properties of wind speed series were focused on hourly or daily averages of wind speed. However, there is no guarantee that the information available for hourly or daily wind speed records can be extended to high-frequency (secondly or less) wind data. It is partly due to instrument constrains. We find that data sets in most previous works are recorded by conventional instruments, *e.g.*, cup or propeller anemometers, which are incapable of measuring turbulence in the natural high-frequency wind speed signals [23]. Using higher frequency sampled data would allow to uncover the complex dynamical behaviors of wind speed at timescales lower than those that have been generally investigated so far [20]. Furthermore, from the methodol-

ogy perspective, in spite of the successful applications of (MF-)DFA noted in the literature [14–20], in the (MF-)DFA method still exist some limitations, which may not be suited for the study of high-frequency wind field, and is in need of further study and refinement. It is partly because the (MF-)DFA method has strict requirements for the data to be investigated and requires basic assumptions, such as the range of timescale and an acceptable level of noise in the signal, which may have difficulty in getting the accurate results [24]. Based on the abovementioned analysis, employing an efficient approach to quantitatively characterize complex dynamical behaviors of high-frequency wind speed would be particularly helpful and necessary.

Quite recently, Gieraltowski *et al.* [24] introduced a method called multi-scale multifractal analysis (MMA), which allows us to extend the description of the properties if the fluctuations of a signal depending on their magnitude and the timescale using the generalized dependence of the local Hurst surface. This method provides a new way of measuring the non-linearity of signals, and has been successfully applied to diverse fields, such as physiological series [24], traffic series [25] and economic series [26].

In this paper, aiming to uncover the non-linear dynamical mechanism underlying high-frequency wind fields, we first systematically carry out an experiment to record nine groups of wind speed data within the atmosphere boundary by using high-precision 2D ultrasonic anemometers. Then, we apply the MMA method to the collected multi-points wind speed data to obtain abundant information about the fractal properties among the entire timescales. Furthermore, we discuss the generating mechanism of multifractality in wind speed time series and the effect of sampling period on the results of MMA. This paper is organized as follows. In Sec. 2, we describe the MF-DFA and MMA methods. In Sec. 3, we briefly introduce the wind speed data used in this study. The results of MMA and some discussions are provided in Sec. 4. Finally, the conclusions are presented in Sec. 5.

2. Methodology

2.1. MF-DFA method

The multifractal detrended fluctuation analysis (MF-DFA) method, developed by Kantelhardt *et al.* [22], is the multifractal extension of the detrended fluctuation analysis (DFA) method [21]. The MF-DFA method is a fairly robust and powerful tool for identifying multifractal characterization of non-stationary time series, and has been widely applied to different fields, such as biology [27], geology [28], economics [29–31], meteorology [14–20]. The MF-DFA algorithm can be briefly described as follows.

Firstly, we consider a time series $x(k)$, $k = 1, 2, \dots, N$, where N is the length of the series. Then, we calculate the integrated series (also called profile)

$$Y(i) = \sum_{k=1}^i (x_k - \bar{x}), \quad i = 1, 2, \dots, N, \quad (1)$$

where $\bar{x} = \frac{1}{N} \sum_{k=1}^N x_k$ is the mean of $x(k)$.

Next, we divide the integrated series into $N_s = \text{int}(N/s)$ non-overlapping segments of equal length s . A short part of the new series $Y(i)$ will remain in most cases because the length N of the series does not have to be a multiple of the considered timescale s . In order not to discard this part of the series, the same procedure is repeated from the other end of the time series. Thus, $2N_s$ segments are obtained altogether.

For each of the $2N_s$ segments, we calculate the local trends by using the k -order polynomial $y_v(i)$ fitting

$$y_v(i) = a_0 + a_1 i + \dots + a_k i^k, \quad k = 1, 2, \dots, \quad (2)$$

where a_k is the polynomial coefficient, k is the order of polynomial fitting. Generally, polynomial detrending of the order of k is capable of eliminating trends up to the order of $k - 1$ [22]. The detrended variance function can be calculated using

$$F^2(s, v) = \frac{1}{s} \sum_{i=1}^s \{Y[(v-1)s+i] - y_v(i)\}^2 \quad (3)$$

for each segment of $v = 1, 2, \dots, N_s$ and

$$F^2(s, v) = \frac{1}{s} \sum_{i=1}^s \{Y[N - (v - N_s)s + i] - y_v(i)\}^2 \quad (4)$$

for each segment of $v = N_s + 1, N_s + 2, \dots, 2N_s$.

According to the above detrending segments, the q order fluctuation function can be obtained by averaging the detrended variance over all segments

$$F_q(s) = \left\{ \frac{1}{2N_s} \sum_{v=1}^{2N_s} [F^2(s, v)]^{q/2} \right\}^{1/q}, \quad (5)$$

where q can take any real value except zero. For $q = 2$, the conventional DFA [21] method is retrieved. For $q = 0$, the fluctuation function $F_0(s)$ can be calculated by

$$F_0(s) = \exp \left\{ \frac{1}{2N_s} \sum_{v=1}^{2N_s} \ln [F^2(s, v)] \right\}. \quad (6)$$

Finally, we determine the scaling behavior of fluctuation function by analyzing the log–log plots $F_q(s)$ versus s for each q

$$F_q(s) \propto s^{h(q)}. \quad (7)$$

The exponent $h(q)$ is called the generalized Hurst exponent. A constant $h(q)$ indicates monofractality, while multifractality is associated with a wide range of values of $h(q)$. For stationary series, $h(2)$ coincides exactly with the Hurst exponent H , *i.e.*, $h(2) = H$ [22]. For non-stationary series but with stationary increments, the relation between $h(2)$ and the Hurst exponent H is $H = h(2) - 1$ [20, 32]. Hurst exponent H is the well-known parameter used to discriminate between persistent/antipersistent/random signals. In particular, $H \in (0, 0.5)$ indicates antipersistency of the time series; $H = 0.5$ indicates uncorrelated noise; $H \in (0.5, 1)$ indicates persistency of the time series.

2.2. MMA method

In previous works, the fluctuation scaling of monofractal series can be characterized by a single exponent, and in most cases, the scaling behavior of multifractal series is described using two-coefficients model. More recently, however, it has been demonstrated many times that the fractal properties vary from point to point along the series and the different scaling exponents are usually required for different parts of the series. Therefore, it is not adequate to illustrate the internal dynamics of signals by using the DFA or MF-DFA method. In order to avoid errors due to improperly predefined scaling ranges, and to obtain all information among the entire timescales, Gieraltowski *et al.* [24] calculated a multifractal spectrum with variable scale ranges and proposed the MMA method. The new technique allows us to investigate not only the multifractal properties but also dependence of these properties on the timescale.

The MMA method is the extension of the MF-DFA method [22]. The process goes like this, after calculating all the q order fluctuation functions $F_q(s)$ by MF-DFA method, we use a moving fitting window, sweeping through all range of the scale s along the $F_q(s)$ plot and obtain a series of overlapped windows. Then, we conduct a fit for points only currently falling into the moving fitting window. In this way, we can study quasi-continuous changes of the $h(q)$ dependence versus the range of scale s . For clarity, we visualize this relationship by the Hurst surface and the points on the surface represent the generalized dependence $h(q, s)$. Since the fluctuation

functions $F_q(s)$ are presented in log–log coordinates, the moving fitting window should expand logarithmically so that it seems to be of constant width. In the original MF-DFA measure, for very small scale, $s < 10$ may result in an arithmetic underflow, for too large scale, usually results in the division of the time series into a too small number of window, which causes the $F_q(s)$ curves to converge at the scale of saturation [24]. Therefore, in this paper, we set the usable scale range for $F_q(s)$ in the MF-DFA procedure to be $s \in [10, 720]$. Next, we set the starting window as scale $s \in [10, 20]$, then move this window at a step of 10, meanwhile expanding the width of the window logarithmically. The ratio between the right endpoint and left endpoint of each expanded window is 2. Thus, we obtain the second window $s \in [20, 40]$, the third window $s \in [30, 60]$, and up to the final window $s \in [360, 720]$, respectively. At last, we calculate the local scaling exponent for each of these windows at different q . The Hurst surface is presented using three linear axes, *i.e.*, order axis (q), scale axis (s), and scaling exponent axis ($h(q, s)$), and the points of the Hurst surface graph are connected to form a colored surface. Note that in the Hurst surface, the scale axis is calibrated so as to show the beginning of each fitting window, that is, it starts from $s = 10$ (*i.e.*, the beginning of the first window [10, 20]) and ends at $s = 360$ (*i.e.*, the beginning of the last window [360, 720]).

Moreover, for multifractal series, the small and large fluctuations scale differently, and there will be a significant dependence of $h(q, s)$ on q . Simply speaking, for positive q , the $h(q, s)$ describes the scaling behavior of the segments with large fluctuations. On the contrary, for negative q , the $h(q, s)$ describes the scaling behavior of the segments with small fluctuations. For monofractal series, the small and large fluctuations scale uniformly and the $h(q, s)$ is independent of q .

3. Experiments and data acquisition

In this paper, the atmospheric boundary-layer turbulence wind speed records, including wind velocity and wind direction, are collected at an open space in the Tianjin University, located at N39.0°, E117.09°. In order to capture the dynamic information of the wind field more comprehensively, nine high-precision 2D Ultrasonic Anemometers (UAs) (WindSonic, Gill Instruments Ltd, sample rate 4 Hz, sound path 0.10 m) are deployed with 5 m interval in a square area and oriented towards the west. The ground surface is flat with smaller roughness. Figure 1 shows the deployment of nine 2D UAs. The measurement height is set as 0.6 m above ground and the recording duration for each measuring location is one hour. Thus, the total number of data points for each UAs is 14 400. These data are applied to analyze the scaling behaviors of the wind speed in the atmospheric boundary layer. Figure 2 illustrates nine groups of wind speed time series recorded at UA_A–UA_I.

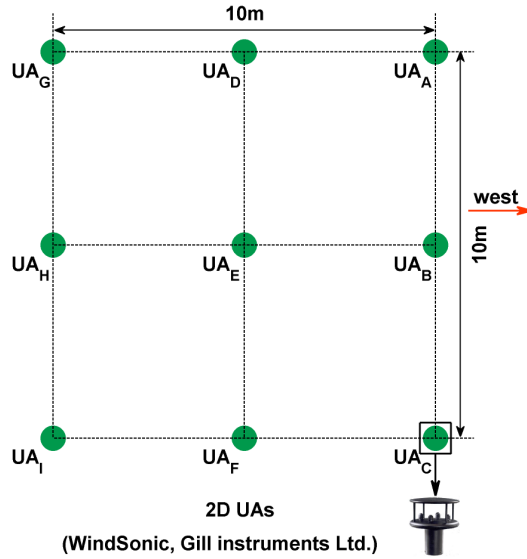


Fig. 1. Deployment of nine 2D ultrasonic anemometers with 4 Hz sampling frequency.

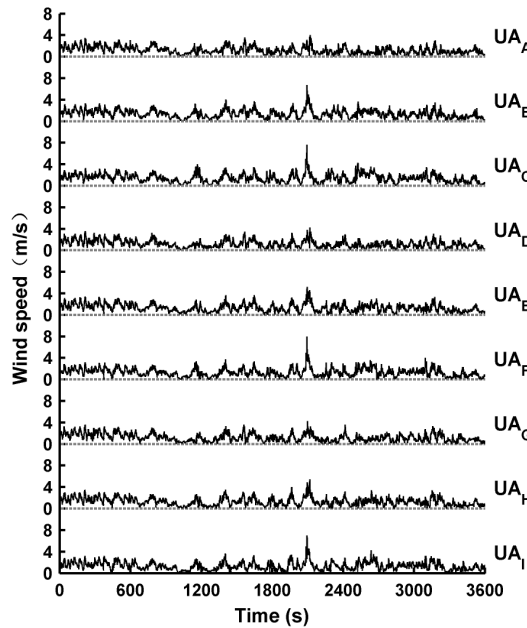


Fig. 2. Nine groups of wind speed time series collected at UA_A – UA_I .

4. Results and analysis

As an example, we first provide MF-DFA results for wind speed time series recorded at UA_A to illustrate the necessity of discussing the multifractal properties within variable scale ranges. Next, the MMA method is applied to characterize the multiscale multifractal properties of nine groups of wind speed data recorded at UA_A – UA_I . Furthermore, the generating mechanism of multifractality of turbulent wind speed is analyzed using shuffling and surrogate techniques. Finally, the effect of sampling period on the MMA results is discussed.

4.1. The necessity of investigation within variable scale ranges for wind speed time series

Figure 3 (a) shows the log–log plot fluctuation functions $F_q(s)$ versus s for the data collected at UA_A . Note that the slopes of the log–log fits to the family of $F_q(s)$ curves determine the Hurst exponent $h(q)$. Therefore, the details of the fitting procedure are crucial to the final results. Instead of the whole scales ($s \in [10, 720]$) used in MF-DFA method, we observe the trend of $h(q)$ with q at different timescales respectively. Figure 3 shows three cases of Hurst curves $h(q)$ for small scales $s \in [10, 20]$, medium scales $s \in [80, 160]$ and large scales $s \in [360, 720]$, respectively. It is obvious that there are different shapes of the $h(q)$ curves for different scale ranges. The values of $h(q)$ for large scales $s \in [360, 720]$ are smaller than those of $h(q)$ for medium

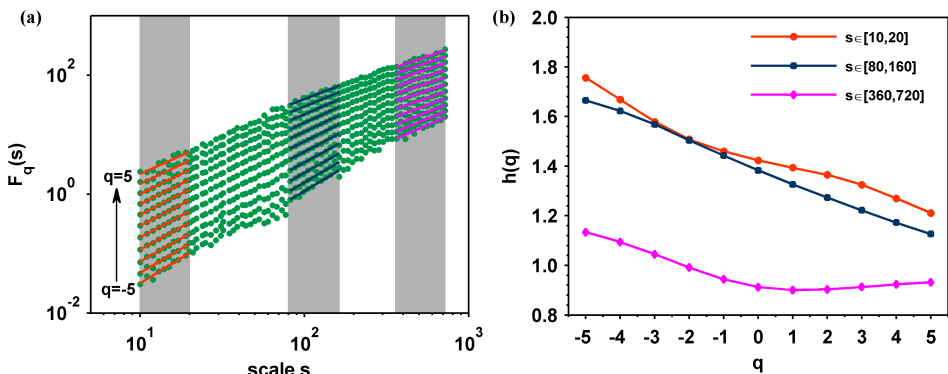


Fig. 3. The multifractal properties of wind speed time series of UA_A . (a) The log–log plot of fluctuation functions $F_q(s)$ versus scale s . The multifractal parameter q is from -5 to 5 with a step of 1 from bottom to top, respectively. The gray areas show three examples of the fitting windows for small scale $s \in [10, 20]$, medium scale $s \in [80, 160]$ and large scale $s \in [360, 720]$. (b) The $h(q)$ curves for $s \in [10, 20]$, $s \in [80, 160]$ and $s \in [360, 720]$, respectively.

and small scales. This analysis indicates that the fractal properties of wind speed records have a relationship with the range of scale s . Likewise, the similar analyses are also performed on the other eight groups of wind speed time series and similar results can be found, which are not shown in this paper for simplicity.

Quite recently, the MMA method has already proven its great potential for obtaining the richer scaling information in time series along the scale ranges and the dynamics of the correlation more fully. Therefore, we employ this state-of-art method, *i.e.*, MMA method, to quantitatively distinguish and uncover the dynamic behaviors underlying high-frequency wind speed time series.

4.2. MMA analysis for high-frequency wind speed data

We first provide the MMA results, *i.e.*, Hurst surface $h(q, s)$, for the data of UA_A as shown in Fig. 4. Compared with the standard MF-DFA, the Hurst surface $h(q, s)$ contains abundant information in which the results of standard MF-DFA can be represented by a single line: a cross section of $h(q, s)$ at a constant s [24]. Furthermore, we find that the Hurst surface $h(q, s)$ of UA_A shows some oscillation at small scales and gradually goes down at large scales. Besides, from the values of $h(2, s)$, we can obtain two timescale ranges of $h(2, s)$: in the higher timescale range ($s > 180$ s), the series is stationary and the values of $h(2, s) \in (0.89, 0.99)$ (which are identical to the Hurst exponent H) indicate that it is characterized by strong persis-

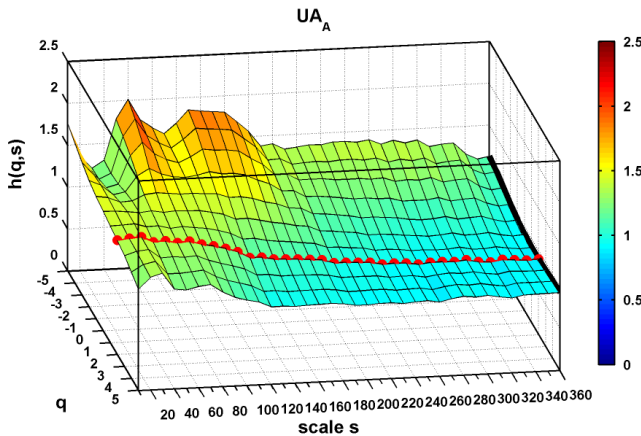


Fig. 4. The Hurst surface $h(q, s)$ dependence calculated for the wind speed records of UA_A . The gray (red) dots show the Hurst curve $h(q, s)$ for $q = 2$, and the black thick line at the right of the plot corresponds to $h(q)$ calculated with the standard MF-DFA method.

tence; in the lower timescale range ($s < 180$ s), the series is non-stationary ($h(2, s) \in (1.02, 1.39)$), and H is $H = h(2, s) - 1 \in (0.02, 0.39)$, which indicates that the series is weakly antipersistent or antipersistent at lower timescales. For a fixed negative q , the curves of $h(q, s)$ experience two rising stages and three dropping stages at small scales and then a stable stage in large scales, while for a fixed positive q , the curves of $h(q, s)$ go through a dropping stage and then a stable stage. It is clear that the fluctuations for negative qs are stronger than those for positive qs . The abovementioned analysis indicates that the MMA method outperforms the MF-DFA technique to characterize the wind speed data.

Next, we turn to focus on the MMA results for nine groups of wind speed data, which are collected simultaneously by nine 2D UAs deployed in the square area with adjacent spacing of 5 m (Fig. 1). Although the nine groups of wind speed data (Fig. 2) look similar, whether multiscale multifractal behaviors for the wind speed data recorded at different positions have spatiotemporal context, it needs further study. Figure 5 provides the Hurst surfaces calculated for nine groups of wind speed data. Note that the Hurst surfaces are placed consistently with the deployment of 2D UAs (Fig. 1).

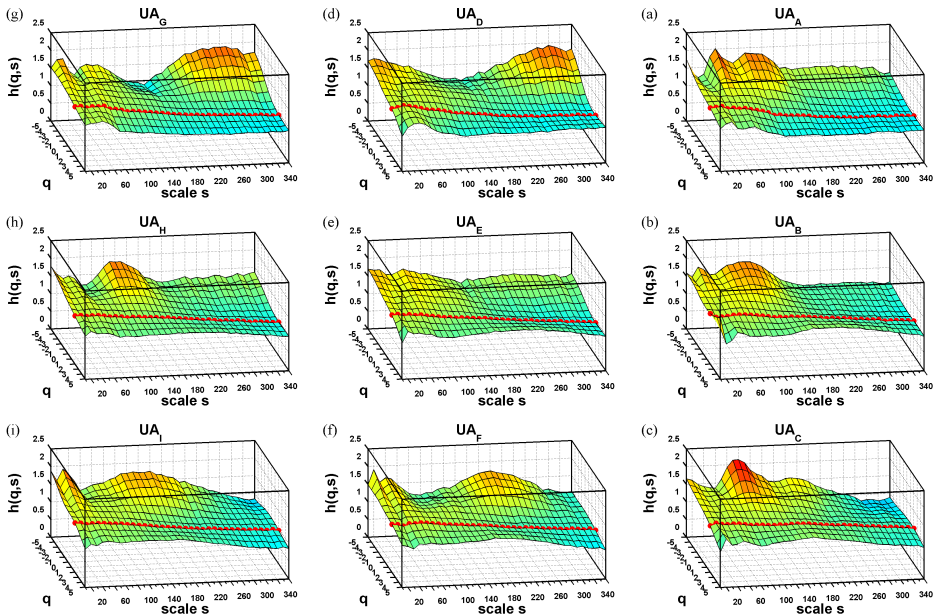


Fig. 5. The Hurst surface $h(q, s)$ dependences calculated for UA_A – UA_I wind speed time series.

Figure 5 shows that the nine Hurst surfaces are dependent upon the order q and timescale s , indicating the necessity of investigating wind speed records from the multiscale perspective. In details, we analyze the curves of $h(q, s)$ from the view point of q and s , respectively. For any fixed scale s , the values of all Hurst surfaces vary with the q , indicating the existence of multifractal properties in all the considered wind speed signals. Meanwhile, all the wind speed series show a more or less intense antipersistence in the lower timescale range and persistence in the higher timescale range, which are deduced by the values of $h(2, s)$. For the positive qs , all the shapes of Hurst surfaces are flat, while for the negative qs , all the surfaces exhibit intensive fluctuations. As mentioned in Sec. 2, for $q > 0$, the $h(q, s)$ describes the scaling behavior of the segments with large fluctuations, while for $q < 0$, the $h(q, s)$ describes the scaling behavior of the segments with small fluctuations. Thus, we can obtain that compared with their large fluctuations behaviors, the small fluctuations of nine groups of wind speed data exhibit more complicated multiscale structure features. Furthermore, for $q < 0$, there are significant differences in all Hurst surfaces, for $q > 0$, all the surfaces look similar, which makes it difficult to distinguish the spatial relationship of UA_A – UA_I wind speed time series.

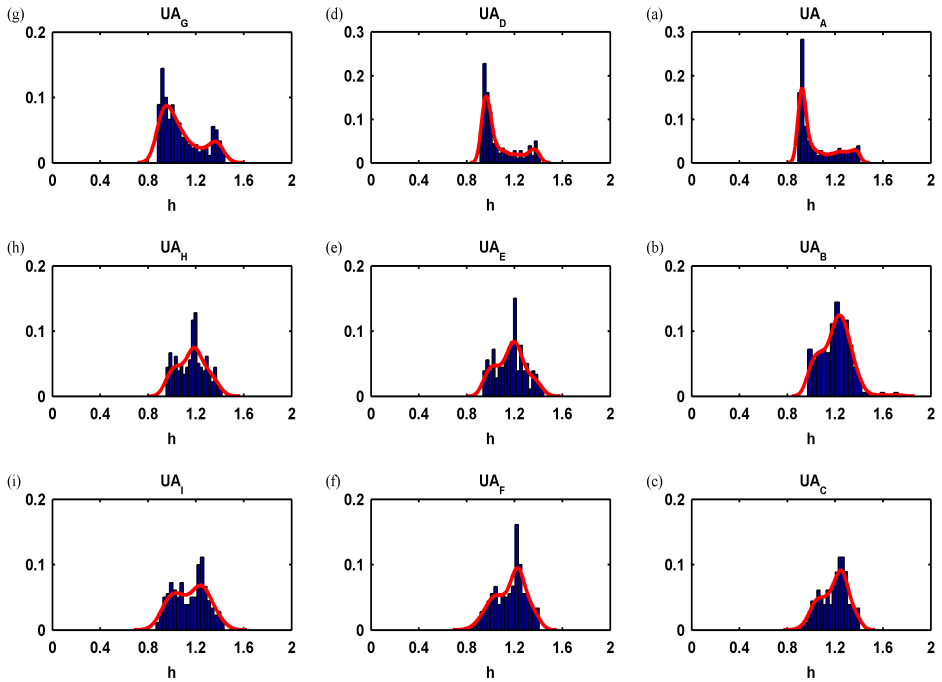


Fig. 6. The histograms of $h(q, s)$ for the nine groups of wind speed time series when q is positive.

In order to further reliably describe the similarities and differences of nine Hurst surfaces for the positive q , we focus on the distribution histograms of Hurst surfaces to quantify the scaling behaviors (Fig. 6). It is obvious that the histograms of Hurst surfaces for the first line (*i.e.*, UA_A , UA_D and UA_G) exhibit similar shapes, indicating similar peaks around $h = 0.9$, however, the histograms for second and third lines show similar behaviors, indicating the similar peaks around $h = 1.2$. These results suggest that the large fluctuations of all wind speed data depend on the spatial positions, which is further illustrated by using the wind roses (Fig. 7). From the wind roses, we can find that the prevailing wind directions are westerly wind, which explains well horizontal not vertical direction similar behaviors in the wind speed records. These interesting findings indicate that the MMA method is very useful for the wind-related researches, including wind field reconstruction and modeling. For example, if we only consider the large fluctuations of nine groups of wind speed data, we can use two 2D UAs to reconstruct the wind field (Fig. 1).

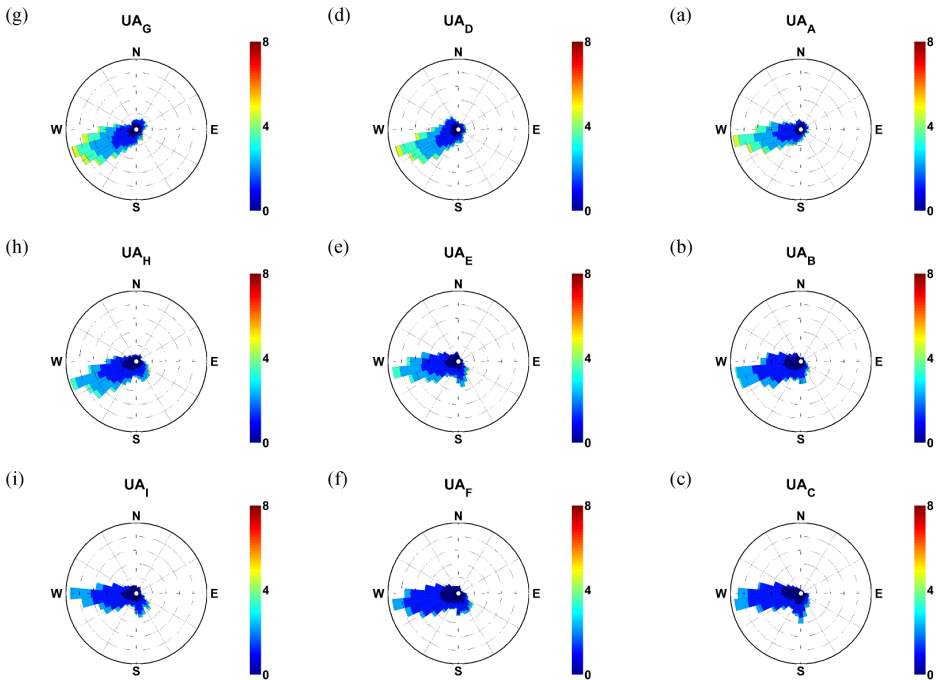


Fig. 7. The wind roses calculated for UA_A – UA_I wind speed time series.

4.3. The generating mechanism of multifractality of wind speed signals

In general, there are two different types of multifractality in the time series [22]: (i) Multifractality due to a broad probability density function for the values of the time series. In this case, the multifractality cannot be removed by shuffling the series. (ii) Multifractality due to different long-range correlations for small and large fluctuations. In this case, the probability density function of the values remains unchanged by shuffling the series, while all long-range correlations are destroyed. Thus, the corresponding shuffled series will exhibit monofractal scaling behavior with Hurst exponent $h_{\text{shuf}}(2) = 0.5$. If both kinds of multifractality are present, the shuffled series will show weaker multifractality than the original series.

To investigate the generating mechanism of multifractality of wind speed signals, we first shuffle the wind speed records (UA_A) to generate a shuffled series. Note that this shuffled series has the identical probability density function with the original series but loses the long-range correlations.

Secondly, we perform a Fourier transform on UA_A wind speed data, preserving the amplitude of the Fourier transform but randomizing the phase, and then perform an inverse Fourier transform. This procedure eliminates non-linearities, preserving only the linear feature of the original series [33]. Thus, we can obtain the corresponding shuffled series and surrogate series [34], respectively. Next, we calculate the generalized Hurst exponent $h(q)$ using the traditional MF-DFA for original series UA_A , shuffled series and surrogate series (Fig. 8 (a) and (c)). One can find that the values of $h_{\text{shuf}}(q)$ are independent of q with a constant value of 0.5, while the values of $h_{\text{sur}}(q)$ have the same varying tendency as the $h(q)$ of original series but are smaller. This result implies that the multifractality of wind speed is due to both long-range correlation and broad probability density function, but is mainly from the long-range correlation.

Furthermore, we compare the Hurst surfaces $h(q, s)$ for the original series with the results of the corresponding shuffled series and surrogate series. We present the average results of 100 realizations of the shuffled and surrogate series (Fig. 8 (b) and (d)). We find that the shuffled procedure apparently destroys the correlations (Fig. 8 (b)), and the Hurst surface $h(q, s)$ of shuffled series is flat ($\langle h_{\text{shuf}}(q, s) \rangle \approx 0.5$). However, the Hurst exponents $h_{\text{sur}}(q)$ of surrogate series vary slightly both with the order q and timescale s ($\langle h_{\text{sur}}(q, s) \rangle \approx 1.19$), as shown in Fig. 8 (d). These findings suggest that the multifractality of wind speed records (UA_A) is due to both long-range correlation and broad probability density function, but the source of multifractality is mainly long-range correlation, which is consistent with the results of MF-DFA. Similar results are obtained for other eight UAs.

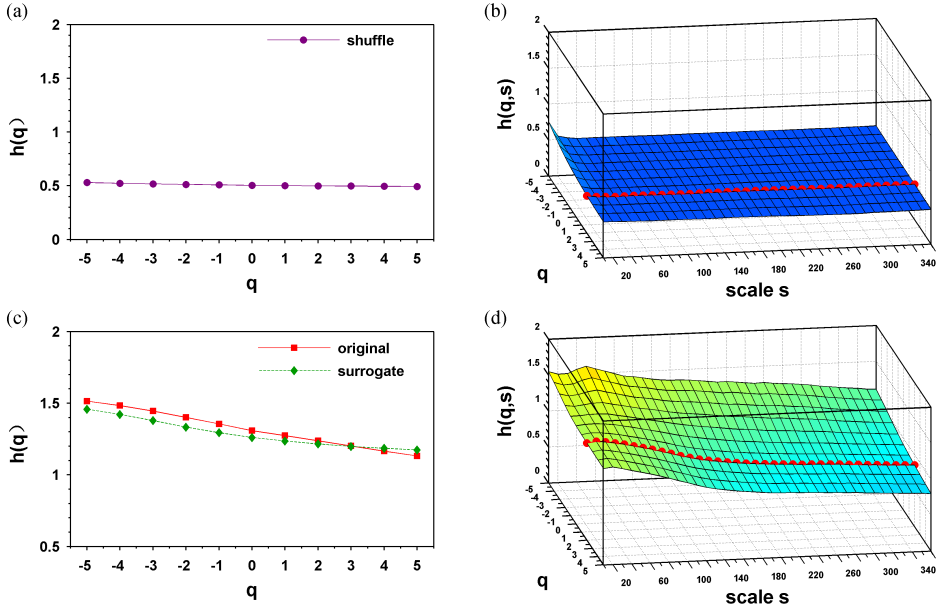


Fig. 8. Comparison of fractal properties for original series (UA_A), shuffled series and surrogate series: (a) and (c) show the results of the standard generalized Hurst exponent $h(q)$ calculated using MF-DFA for three kinds of series; (b) and (d) show the Hurst surface $h(q, s)$ calculated using MMA for shuffled and surrogate series, respectively.

4.4. Effect of sampling period

The sampling period is an important consideration for defining the scales of turbulence. This issue is easily overlooked and encountered during experimental planning and may affect the accuracy of measurement of flow properties in complex, natural flows [23]. For instance, if the sampling period is too short, the largest eddies may not be captured and included in Reynolds stress estimates. Boxel *et al.* [35] suggested that for measurements below 1.0 m height, if the sampling period is taken too long (*e.g.* longer than 60 min), the trends resulting from the daily course start influencing the results. Thus, in our work, the sampling period for all the UAs is one hour, which is adequate both for eliminating daily trend and measuring turbulence. To find out what effect has the sampling period on the MMA results, we select four groups of test series in which the sampling periods are 30 min, 20 min, 15 min and 10 min. The starting points of the subseries are the same, *i.e.*, the first point of the original series. The corresponding results of Hurst surfaces are provided in Figs. 9, 10, 11 and 12, respectively.

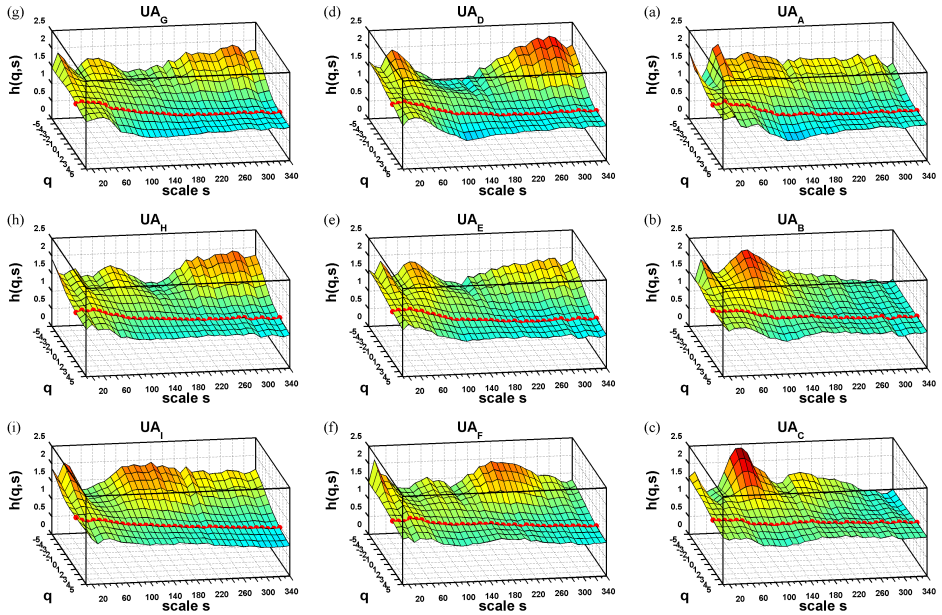


Fig. 9. The Hurst surfaces calculated for UA_A – UA_I with 30 min sampling period.

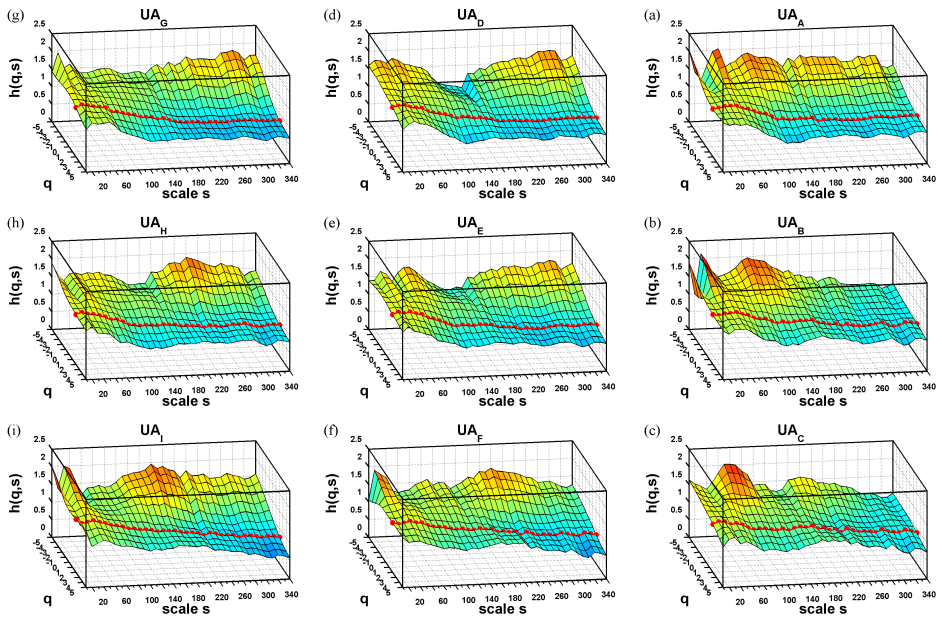


Fig. 10. The Hurst surfaces calculated for UA_A – UA_I with 20 min sampling period.

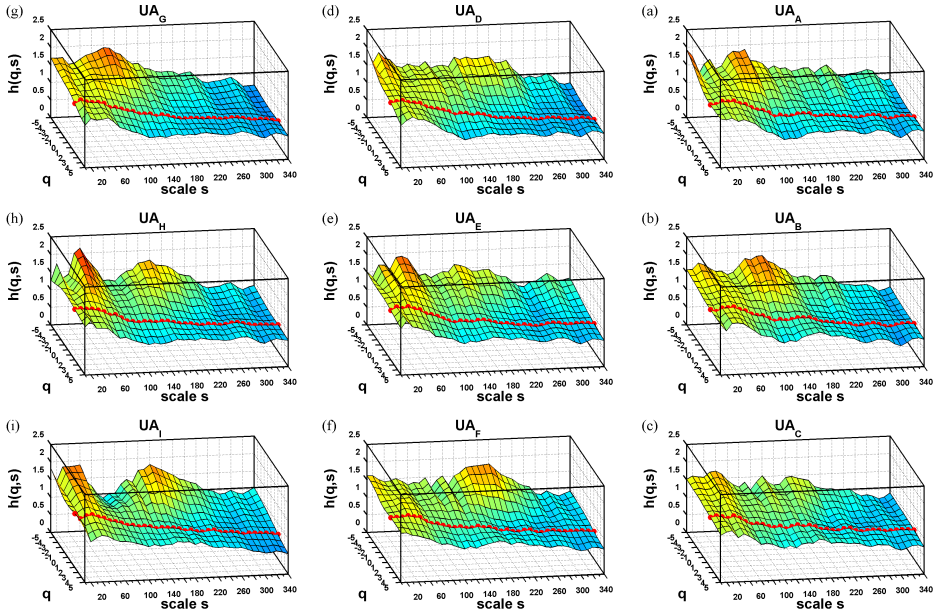


Fig. 11. The Hurst surfaces calculated for UA_A – UA_I with 15 min sampling period.

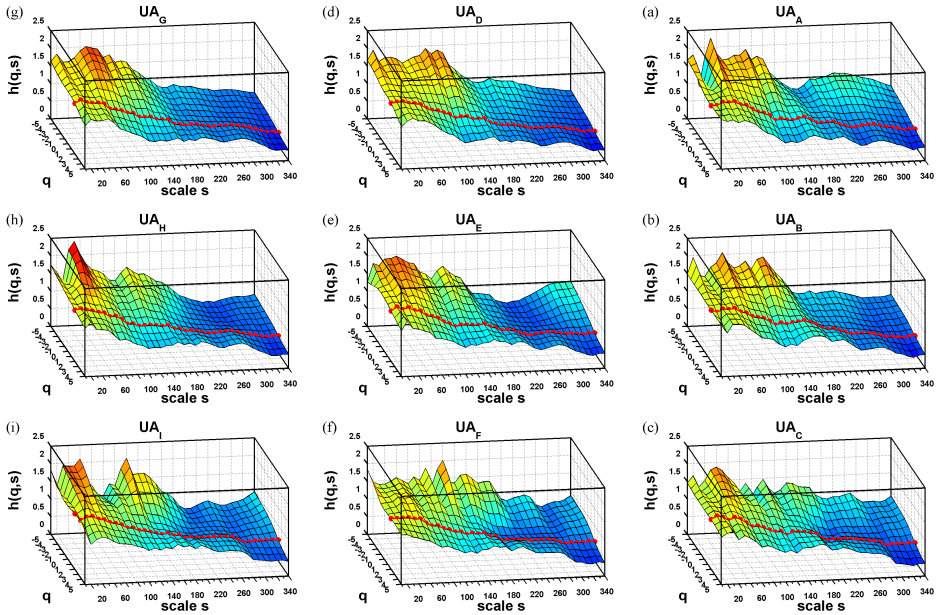


Fig. 12. The Hurst surfaces calculated for UA_A – UA_I with 10 min sampling period.

Next, we employ the intersurface distance to reliably describe and quantify the differences between original one-hour series and 30 min, 20 min, 15 min, 10 min series, respectively. The intersurface distance between $h_1(q, s)$ and $h_2(q, s)$ can be calculated by using the following equations [24]:

$$h_{2s}(q, s) = h_2(q, s) + [\langle h_1(q, s) \rangle - \langle h_2(q, s) \rangle], \tag{8}$$

$$d = \left\{ \langle [h_1(q, s) - h_{2s}(q, s)]^2 \rangle \right\}^{1/2} [\langle h_1(q, s) \rangle]^{-1}, \tag{9}$$

where $h_1(q, s)$ is a reference surface, d is a measure of the mean distance between two Hurst surfaces $h_1(q, s)$ and $h_2(q, s)$, and $\langle \bullet \rangle$ denotes the mean. In this study, we set the threshold $d = 0.10$. If $d \leq 0.10$, we consider the shape of two surfaces to be similar, and if $d \geq 0.10$, we consider them to be different.

Table I shows that the intersurface distances between original one-hour series and the series of 30 min and 20 min are below the threshold 0.1, indicating that those three wind speed series possess similar scaling behaviors (see Figs. 5, 9 and 10). However, all distances are larger than 0.1 when sampling periods are set as 15 min and 10 min (Figs. 11 and 12). In addition, one can see that the shapes of the nine Hurst surfaces look similar when the sampling period is 10 min (Fig. 12). These results suggest that in order to obtain abundant scaling information of high-frequency wind speed records, the sampling period should be not less than 20 min, which is in agreement with the result in [35].

TABLE I

Intersurface distances between original series of one-hour sampling period and 30, 20, 15 and 10 min series.

Wind speed	Distance			
	30 min	20 min	15 min	10 min
UA _A	0.0735	0.0944	0.1022	0.1642
UA _B	0.0825	0.0970	0.1270	0.1924
UA _C	0.0713	0.0942	0.1236	0.1863
UA _D	0.0807	0.0927	0.2142	0.2972
UA _E	0.0707	0.0736	0.1314	0.2147
UA _F	0.0780	0.0986	0.1155	0.2273
UA _G	0.0715	0.0949	0.2554	0.3237
UA _H	0.0999	0.1000	0.1808	0.2420
UA _I	0.0933	0.0956	0.1200	0.1992

5. Conclusions

In this study, the high-frequency wind speed signals recorded at different spatial positions are examined using the generalized dependence of the local Hurst exponent on the scale: the surface $h(q, s)$. We concentrate not only on the fact that the high-frequency wind speed records have multifractal properties but also these properties depend on the timescale.

The results of log–log plot fluctuation functions $F_q(s)$ show that the multifractal properties of wind speed data have a relationship with the range of scale s , indicating the limitation of traditional multifractal detrended fluctuation analysis (MF-DFA) method using a fixed timescale. Then, we systematically investigate the dynamic behaviors of the small fluctuations and large fluctuations in nine groups of high-frequency wind speed data, applying the MMA method. The results of Hurst surfaces reveal that for the negative qs , all the surfaces exhibit intensive fluctuations and there are significant differences. Meanwhile, the distribution histograms of Hurst surfaces for the positive qs suggest that the large fluctuations of all wind speed data depend on the spatial positions, *i.e.*, horizontal not vertical direction similar relationship, which is further illustrated by the wind roses. Furthermore, it is demonstrated that the multifractality of wind speed time series is due to both long-range correlation and broad probability density function, but the long-range correlation is the main source, via comparing the original series with their shuffled and surrogate series. Finally, we discuss the effect of sampling period on the MMA results. It is observed that the MMA results with sampling period of series from 30 min to 20 min are consistent with the original series for one-hour sampling period, while some deviations occur when the sampling period is lower than 20 min. This result reveals that a sampling period of 20 min is sufficient to characterize multiscale multifractal properties of high-frequency wind speed data.

However, there are still some issues that need further study. For example, we can use the cross correlation analysis methods [36–38] to investigate the spatiotemporal relationships of wind speed signals recorded at different positions. Furthermore, some interesting findings can be used to develop theoretical and computational models for various wind-related phenomena, *e.g.*, wind field reconstruction and wind pattern recognition.

This work was supported in part by the National Natural Science Foundation of China under grant Nos. 61271321, 61573253, 61401303, Tianjin Key Technology Research and Development Program (14ZCZDSF00025), Tianjin Natural Science Foundation under grant No. 13 JCYBJC17500, Doctoral Fund of Ministry of Education of China under grant No. 20120032110068.

REFERENCES

- [1] B.C. Ummels *et al.*, *IEEE Trans. Energ. Convers.* **22**, 44 (2007).
- [2] E. Demirci, B. Cuhadaroglu, *Energy Buildings* **31**, 49 (2000).
- [3] J.E. Cermak, *J. Wind Eng. Ind. Aerodyn.* **91**, 355 (2003).
- [4] G. Sterk *et al.*, *Earth Surf. Proc. Land.* **23**, 877 (1998).
- [5] R.G. Kavasseri, R. Nagarajan, *IEEE Trans. Circuits Syst. I* **51**, 2255 (2004).
- [6] M.R. Raupach, A.S. Thom, I. Edwards, *Bound-Lay. Meteorol.* **18**, 373 (1980).
- [7] D.R. Parsons, I.J. Walker, G.F.S. Wiggs, *Geomorphology* **59**, 149 (2004).
- [8] A.N. Celik, *Renewable Energy* **29**, 593 (2004).
- [9] T.E. Karakasidis, A. Charakopoulos, *Chaos Soliton Fract.* **41**, 1723 (2009).
- [10] S. Avdakovic *et al.*, *Int. J. Environ. Chem. Ecol. Geol. Geophys. Eng.* **5**, 138 (2011).
- [11] V.D.H. Isaac, *J. Meteorol.* **14**, 160 (1957).
- [12] S. Alpay *et al.*, *Int. J. Energ. Res.* **30**, 359 (2006).
- [13] Z.T. Fu *et al.*, *Commun. Nonlinear Sci.* **19**, 83 (2014).
- [14] R.G. Kavasseri, R. Nagarajan, *Chaos Soliton Fract.* **24**, 165 (2005).
- [15] R.G. Kavasseri, R. Nagarajan, *Fluct. Noise Lett.* **6**, 201 (2006).
- [16] K. Koçak, *Energy* **34**, 1980 (2009).
- [17] M.D.O. Santos, T. Stosic, B.D. Stosic, *Physica A* **391**, 1546 (2012).
- [18] T. Feng, Z.T. Fu, J.Y. Mao, *Phys. Lett. A* **373**, 4134 (2009).
- [19] L. Telesca, M. Lovallo, *J. Stat. Mech.* **2001**, P07001 (2011).
- [20] L. Telesca, M. Lovallo, M. Kanevski, *Appl. Energy* **162**, 1052 (2016).
- [21] C.K. Peng *et al.*, *Phys. Rev. E* **49**, 1685 (1994).
- [22] J.W. Kantelhardt *et al.*, *Physica A* **316**, 87 (2002).
- [23] I.J. Walker, *Geomorphology* **68**, 57 (2005).
- [24] J. Gieraltowski, J.J. Żebrowski, R. Baranowski, *Phys. Rev. E* **85**, 021915 (2012).
- [25] J. Wang, P.J. Shang, X.R. Cui, *Phys. Rev. E* **89**, 032916 (2014).
- [26] A.J. Lin, H. Ma, P.J. Shang, *Physica A* **436**, 525 (2015).
- [27] R. Magrans *et al.*, *Physiol. Meas.* **31**, 565 (2010).
- [28] L. Telesca *et al.*, *Tectonophysics* **642**, 71 (2015).
- [29] Y.P. Tuan, W.X. Zhou, *Physica A* **390**, 1646 (2011).
- [30] M. Bolgorian, Z. Gharli, *Acta Phys. Pol. B* **42**, 159 (2011).
- [31] D. Ghosh, S. Dutta, S. Samant, *Acta Phys. Pol. B* **43**, 1261 (2012).
- [32] M. Sadegh Movahed *et al.*, *J. Stat. Mech.* **2006**, P02003 (2006).
- [33] P.C. Ivanov *et al.*, *Nature* **399**, 461 (1999).

- [34] J. Theiler *et al.*, *Phys. D* **58**, 77 (1992).
- [35] J.H. van Boxel *et al.*, *Geomorphology* **59**, 131 (2004).
- [36] W.X. Zhou, *Phys. Rev. E* **77**, 066211 (2008).
- [37] Z.Q. Jiang, W.X. Zhou, *Phys. Rev. E* **84**, 016106 (2011).
- [38] Y. Yin, P.J. Shang, *Nonlinear Dynam.* **81**, 1329 (2015).